



ORIGINAL RESEARCH COMMUNICATION

# Knockout of Mitochondrial Thioredoxin Reductase Stabilizes Prolyl Hydroxylase 2 and Inhibits Tumor Growth and Tumor-Derived Angiogenesis

Juliane Hellfritsch,<sup>1,\*</sup> Julian Kirsch,<sup>1,\*</sup> Manuela Schneider,<sup>1</sup> Tamara Fluege,<sup>2</sup> Markus Wortmann,<sup>1</sup> Jeroen Frijthoff,<sup>3</sup> Markus Dagnell,<sup>3</sup> Theres Fey,<sup>1</sup> Irene Esposito,<sup>4,5</sup> Pirkko Kölle,<sup>6</sup> Kristin Pogoda,<sup>1</sup> José Pedro Friedmann Angeli,<sup>7</sup> Irina Ingold,<sup>7</sup> Peter Kuhlencordt,<sup>6</sup> Arne Östman,<sup>3</sup> Ulrich Pohl,<sup>1</sup> Marcus Conrad,<sup>2,7</sup> and Heike Beck<sup>1</sup>

## Abstract

**Aims:** Mitochondrial thioredoxin reductase (Txnrd2) is a central player in the control of mitochondrial hydrogen peroxide (H<sub>2</sub>O<sub>2</sub>) abundance by serving as a direct electron donor to the thioredoxin-peroxiredoxin axis. In this study, we investigated the impact of targeted disruption of Txnrd2 on tumor growth. **Results:** Tumor cells with a Txnrd2 deficiency failed to activate hypoxia-inducible factor-1 $\alpha$  (Hif-1 $\alpha$ ) signaling; it rather caused PHD2 accumulation, Hif-1 $\alpha$  degradation and decreased vascular endothelial growth factor (VEGF) levels, ultimately leading to reduced tumor growth and tumor vascularization. Increased c-Jun NH2-terminal Kinase (JNK) activation proved to be the molecular link between the loss of Txnrd2, an altered mitochondrial redox balance with compensatory upregulation of glutaredoxin-2, and elevated PHD2 expression. **Innovation:** Our data provide compelling evidence for a yet-unrecognized mitochondrial Txnrd-driven, regulatory mechanism that ultimately prevents cellular Hif-1 $\alpha$  accumulation. In addition, simultaneous targeting of both the mitochondrial thioredoxin and glutathione systems was used as an efficient therapeutic approach in hindering tumor growth. **Conclusion:** This work demonstrates an unexpected regulatory link between mitochondrial Txnrd and the JNK-PHD2-Hif-1 $\alpha$  axis, which highlights how the loss of Txnrd2 and the resulting altered mitochondrial redox balance impairs tumor growth as well as tumor-related angiogenesis. Furthermore, it opens a new avenue for a therapeutic approach to hinder tumor growth by the simultaneous targeting of both the mitochondrial thioredoxin and glutathione systems. *Antioxid. Redox Signal.* 22, 938–950.

## Introduction

**D**URING TUMOR GROWTH, an increase in the levels of intracellular reactive oxygen species (ROS) is commonly observed (30). However, protective enzymatic antioxidant systems are upregulated, simultaneously (6). Accordingly, these antioxidant systems have been sug-

gested as targets for redox-dependent anti-cancer treatment (47).

In mammalian cells, the major intracellular sites for ROS production are the mitochondria, in which leakage of electrons generates superoxide that is readily dismutated by superoxide dismutase to hydrogen peroxide (H<sub>2</sub>O<sub>2</sub>). To maintain ROS at nonpathological levels, cells are equipped

<sup>1</sup>Walter Brendel Centre of Experimental Medicine, Munich Heart Alliance, Ludwig-Maximilians-University, Munich, Germany.

<sup>2</sup>Institute of Clinical Molecular Biology and Tumor Genetics, Helmholtz Zentrum München, German Research Center for Environmental Health, Munich, Germany.

<sup>3</sup>Department of Oncology and Pathology, Cancer Center Karolinska, Karolinska Institutet, Stockholm, Sweden.

<sup>4</sup>Institute of Pathology, Helmholtz Zentrum München, German Research Center for Environmental Health, Neuherberg, Germany.

<sup>5</sup>Institute of Pathology, Technische Universität München, Munich, Germany.

<sup>6</sup>Department of Vascular Medicine, Medizinische Klinik und Poliklinik IV, Klinikum der Universität München, Munich, Germany.

<sup>7</sup>Institute of Developmental Genetics, Helmholtz Zentrum München, Neuherberg, Germany.

\*Equal contribution.

**Innovation**

Investigations regarding the role of reactive oxygen species (ROS) in PHD2 stabilization and thus hypoxia-inducible factor-1 $\alpha$  (Hif-1 $\alpha$ ) signaling in tumor development have yielded controversial results. Taking advantage of well-defined knockout tumor models, evidence is provided that the chronic leakage of mitochondrial ROS triggers PHD2 stabilization in a JNK-dependent manner that, ultimately, leads to impaired tumor angiogenesis and tumor growth. This study highlights the relevance of mitochondrial thioredoxin reductase as a yet-unrecognized critical player in tumor development.

with highly efficient antioxidant redox networks. With regard to mitochondrial redox homeostasis, the peroxiredoxin III (Prx III)/mitochondrial thioredoxin (Txn2)/mitochondrial thioredoxin reductase (Txnrd2) axis is considered the most important H<sub>2</sub>O<sub>2</sub>-scavenging system (14, 45), as corroborated by reverse genetics in mice: Mice lacking Prx III are viable but show increased sensitivity to ROS-generating toxins (29); genetic deletion of either *Txn2* or *Txnrd2* causes embryonic lethal phenotypes during mid-gestation and fetal development, respectively (10, 36).

Hypoxia is another classical hallmark of tumor growth and metastasis (21). The individual components of hypoxic signaling downstream of restricted oxygen and nutrient supply are well established and comprise the inactivation of Hypoxia-inducible factor prolyl hydroxylase (PHD) and subsequent stabilization of Hypoxia-inducible factor-1 $\alpha$  (Hif-1 $\alpha$ ), culminating in increased transcription of Hif-1 $\alpha$  target genes (41). *Via* these target genes, Hif-1 $\alpha$  is involved in a myriad of cellular processes, including typical features favoring tumor growth such as angiogenesis or cell proliferation (44, 53). Interestingly, Hif-1 $\alpha$  can also be stabilized under nonhypoxic conditions in response to various hormones (19), growth factors, and cytokines (23), and many of these stimuli induce ROS production as a part of their signaling cascade. Although the role of hypoxia in tumor growth is well established, conclusive data on the contribution of cellular ROS to hypoxic signaling are scarce and even conflicting. Previously, H<sub>2</sub>O<sub>2</sub> was viewed as an inevitable and toxic by-product of aerobic life due to its potentially deleterious side effects. A number of studies, however, suggest that H<sub>2</sub>O<sub>2</sub> plays an important role in cell signaling by regulating a diverse set of physiological processes (12). Previous reports demonstrated that Hif-1 $\alpha$  stabilization and activation of its target genes can also be induced by exogenous H<sub>2</sub>O<sub>2</sub> or other oxidative stressors (4, 8, 15, 34). Furthermore, mitochondrial ROS production has also been shown to stabilize Hif-1 $\alpha$  (5, 20, 34), and Hif-1 $\alpha$  DNA-binding activity appears to be sensitive to oxidizing reagents (51). On the other hand, short pre-exposure of cells to H<sub>2</sub>O<sub>2</sub> selectively prevents hypoxia-induced Hif-1 $\alpha$  binding by preventing the accumulation of Hif-1 $\alpha$  protein, whereas treatment of hypoxic cell extracts with H<sub>2</sub>O<sub>2</sub> has no effect on Hif-1 $\alpha$  binding (24). It appears that ROS can interfere with the Hif-1 $\alpha$  pathway at the level of PHDs by oxidizing the essential co-factor ferrous iron [Fe(II)] to the inactive ferric form [Fe(III)] (17, 38). However, to date, the precise link between ROS and hypoxic signaling has remained elusive.

To address whether the PrxIII/Txn2/Txnrd2 axis contributes to tumor growth/viability by maintaining redox ho-

meostasis and controlling hypoxic signaling, we generated transformed cells with a targeted deficiency in the mitochondrial ROS-regulating enzyme Txnrd2.

In our experiments, we could show that loss of Txnrd2 in tumor cells results in a modified cellular redox balance. This imbalance leads to a sustained upregulation of PHD2 and failure to stabilize Hif-1 $\alpha$  even in response to appropriate stimuli, ultimately culminating in the inhibition of tumor vascularization and growth. We additionally identified c-Jun NH2-terminal Kinase (JNK) as a hitherto unknown participant in ROS-mediated hypoxic signaling.

**Results***Transformation and characterization of Txnrd2-deficient mouse embryonic fibroblasts*

The gene targeting strategy for the disruption of *Txnrd2* is depicted in Figure 1A (10). First, mouse embryonic fibroblasts (MEFs) were isolated from E12.5 embryos. Genotyping and immunoblotting was performed to confirm the deletion of *Txnrd2* (Fig. 1B). To maintain H<sub>2</sub>O<sub>2</sub> emission from the mitochondria at cell-tolerable levels, *Txnrd2*<sup>-/-</sup> MEFs responded with a strong compensatory upregulation of the mitochondria-located oxidoreductase glutaredoxin-2 (*grx2*) ( $n=5$ , Fig. 1C). However, despite this compensatory response, *Txnrd2*<sup>-/-</sup> cells still displayed higher ROS levels than wild-type (WT) cells (mean fluorescence intensity:  $8.6 \pm 2.1$  in *Txnrd2*<sup>+/+</sup> vs.  $25.2 \pm 7.6$  in *Txnrd2*<sup>-/-</sup> cells,  $n=10$ , Fig. 1D).

Immortalized MEFs were transformed by lentiviral transduction of the proto-oncogene c-Myc and the oncogene Ha-ras<sup>V12</sup> and plated in soft agar (28). We established transformed cell lines from individually picked clones. This was deemed necessary as a basis for the *in vivo* tumor cell implantation studies. Equal expression of c-Myc and Ha-ras<sup>V12</sup> was confirmed by immunoblotting (Fig. 1E). Transformation of cells did not have any impact on cellular ROS levels (mean fluorescence intensity:  $9.9 \pm 1.6$  in *Txnrd2*<sup>+/+</sup> vs.  $20.7 \pm 4.9$  in *Txnrd2*<sup>-/-</sup>,  $n=10$ , data not shown). However, we observed an alignment of *in vitro* proliferation of the transformed WT and knockout (KO) clones under baseline cell culture conditions ( $n=6$ , Fig. 1F).

Since the Prx III-dependent release of H<sub>2</sub>O<sub>2</sub> from the mitochondria is not only under the control of the Trx2-Txnrd2 node but can also be altered by *grx2* in a glutathione (GSH)-dependent manner (22), we tested how *Txnrd2*-deficient cells would react to an additional loss of GSH. Indeed, when *Txnrd2*<sup>-/-</sup> cells were treated with L-buthionine sulfoximine (BSO), a highly specific and irreversible inhibitor of the GSH-synthesizing enzyme  $\gamma$ -glutamylcysteine synthetase, cell survival and proliferation were considerably impaired ( $n=6$ , Fig. 1G).

*Targeted loss of Txnrd2 substantially impairs tumor growth in vivo*

Having been characterized, transformed cells were subcutaneously implanted into the retrol flank of C57BL/6 mice. Although single cell-derived transformed fibroblasts showed no difference in proliferation rates *in vitro* ( $n=6$ , Fig. 1F), the tumor mass of tumors formed by *Txnrd2*-deficient cells was substantially reduced by  $\sim 50\%$  (mean  $0.8 \pm 0.16$  g, median

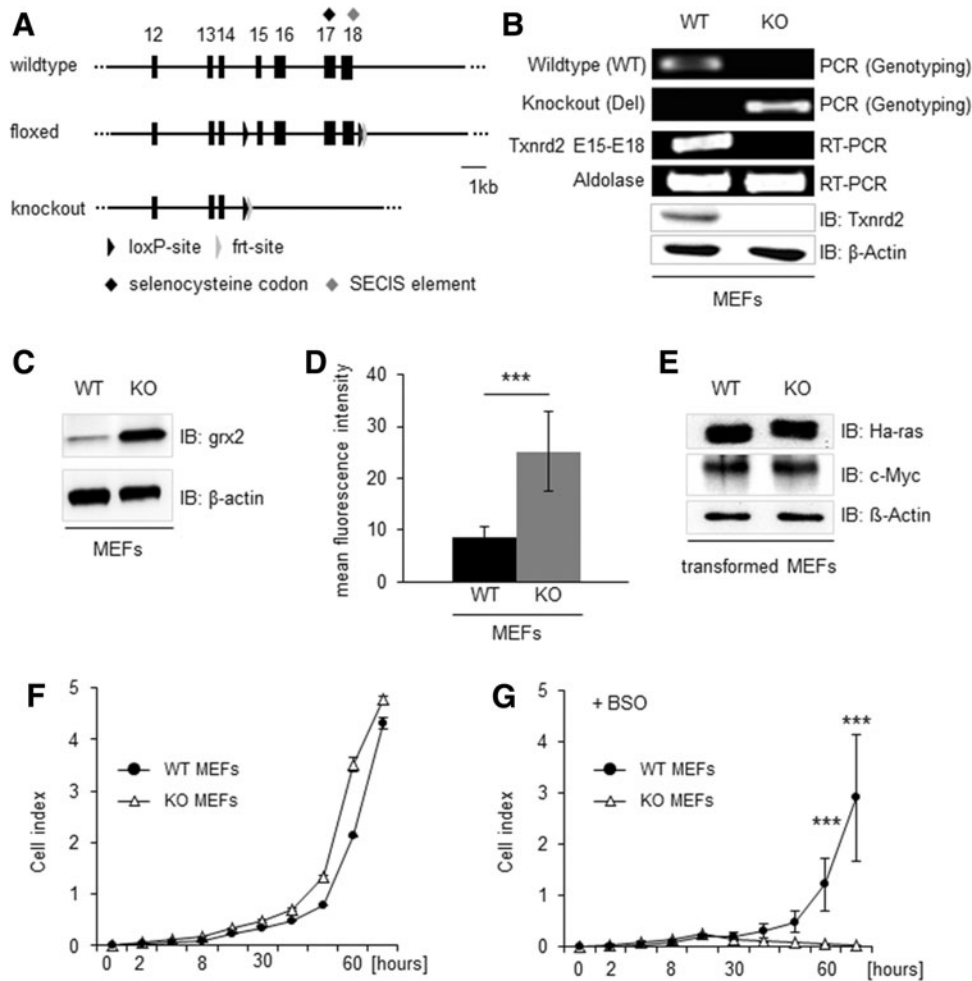


**FIG. 1. Targeted loss of *Txnrd2* and its effects on cellular redox balance.** (A) Schematic outline of the generation of the conditional *Txnrd2* knockout (KO) allele (10). (B) Expression of *Txnrd2* in MEFs was analyzed on the genomic (*top panels*), mRNA (*middle panels*) as well as at the protein level (*bottom panels*). Equal loading was confirmed by *Aldolase* or  $\beta$ -Actin expression. (C) Immunoblot revealed that *grx2* expression levels are strongly upregulated in *Txnrd2*<sup>-/-</sup> MEFs. (D) Total cellular ROS levels were determined by flow cytometry using the fluorogenic probe CellROX Deep Red Reagent. Note that despite the enhanced levels of *grx2* expression, *Txnrd2*-deficient MEFs accumulate more ROS than wild-type (WT) cells. (E) Equal expression of c-Myc and Ha-ras in transformed *Txnrd2*<sup>+/+</sup> and *Txnrd2*<sup>-/-</sup> cells was confirmed by immunoblotting. (F) The proliferation rate of transformed *Txnrd2*<sup>-/-</sup> MEFs (KO) is similar to that of WT cells. (G) Transformed *Txnrd2*<sup>-/-</sup> cells are sensitive to cell death induced by GSH depletion in contrast to WT cells. Data in (D) are represented as mean  $\pm$  SD, data in (F, G) as mean  $\pm$  SEM. \*\*\**p* < 0.001. *grx2*, glutaredoxin-2; MEFs, mouse embryonic fibroblasts; ROS, reactive oxygen species; RT-PCR, real-time-polymerase chain reaction; SD, standard deviation.

0.6 g) after 11 days in contrast to tumors from *Txnrd2*-expressing cells (mean  $1.7 \pm 0.34$  g, median 1.57 g, *n* = 25, Fig. 2A). Analysis of tumor growth at different time points indicated that the difference in the tumor mass was most pronounced on day 11 (day 2, *n* = 3; day 3, *n* = 9; day 4, *n* = 3; day 6, *n* = 9, day 8, *n* = 3; day 11, *n* = 25, Fig. 2B).

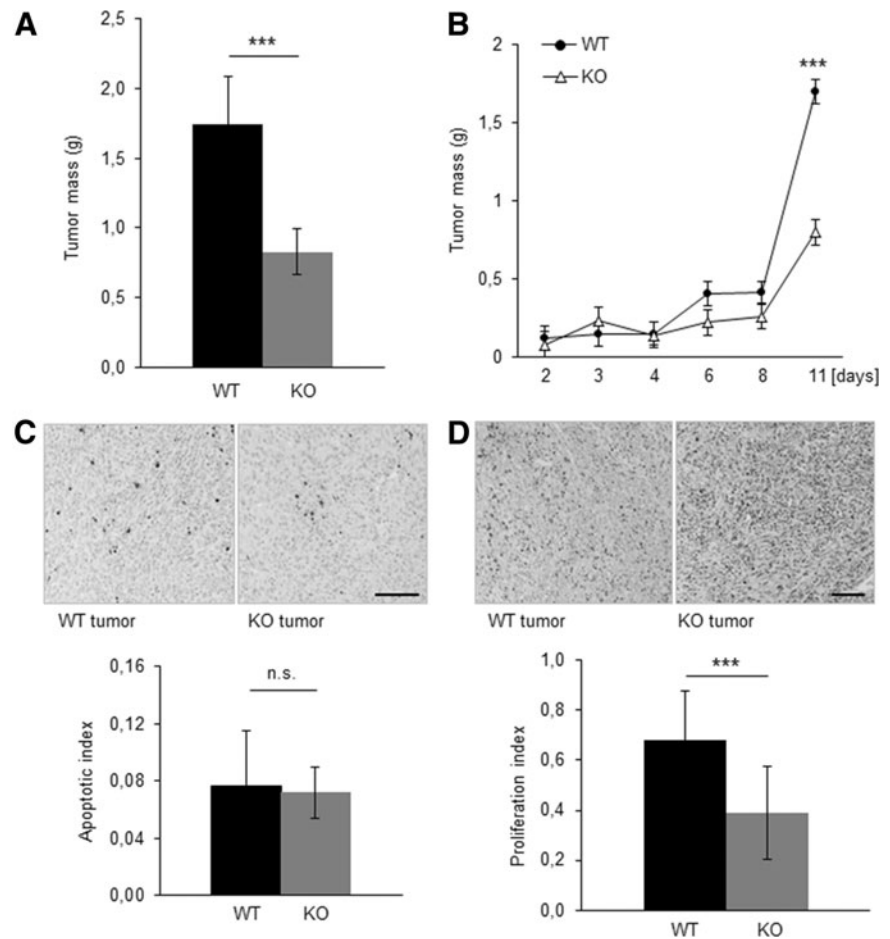
Histological analysis was performed to elucidate the underlying reasons for the attenuated tumor growth. Quantification of cells positive for cleaved caspase-3, an apoptosis marker, revealed no difference (*Txnrd2*<sup>+/+</sup>  $0.08 \pm 0.1$  vs. *Txnrd2*<sup>-/-</sup>  $0.07 \pm 0.05$  positive cells per region of interest, [Fig. 2C]). The assessment of necrotic areas within the tumors (*n* = 6) also revealed that the smaller tumor volume was not a result of necrotic cell loss (percentage of the necrotic area relative to the entire tumor area: *Txnrd2*<sup>+/+</sup> tumors:  $20\% \pm 6.5\%$  vs. *Txnrd2*<sup>-/-</sup> tumors:  $14.5\% \pm 7.2\%$ , data not

shown). However, *Txnrd2*-deficient tumors immunostained for the proliferation marker Ki-67 showed a significantly lower ratio of proliferating to nonproliferating cells (proliferation index [PI]) than WT tumors ( $0.39 \pm 0.19$  vs.  $0.68 \pm 0.14$ , *n* = 6 tumors per group, Fig. 2D).

#### *Txnrd2*<sup>-/-</sup> tumors are highly susceptible to pharmacologic GSH deprivation

In our initial *in vitro* experiments, we could show that depletion of GSH by BSO resulted in the death of *Txnrd2*-deficient cells (Fig. 1G). Since both *Txnrd2* and *grx2* contribute to the reduction of Prx III (22), thereby controlling H<sub>2</sub>O<sub>2</sub> emission from the mitochondria, we assessed whether inhibition of the *de novo* GSH synthesis may represent a pharmacological rationale to further reduce the growth of

**FIG. 2. Loss of *Txnrd2* results in a strong reduction in tumor growth.** (A) Subcutaneous injection of single-cell-derived transformed cells into C57BL/6 mice revealed a substantial reduction of tumor growth in *Txnrd2* null tumors. (B) A longitudinal determination of tumor mass indicated that tumor weight differences were most pronounced at day 11. (C, D) While the number of cells positive for cleaved caspase-3 (apoptotic cells) was not different among the groups at day 11 (C), the number of proliferating, Ki-67-positive cells was strongly reduced in *Txnrd2* null tumors (D). \*\*\* $p < 0.001$ . Data are represented as mean  $\pm$  SD. n.s., not significant. Scale bar = 100  $\mu$ m.



*Txnrd2*-deficient tumors *in vivo*. First, we confirmed that *Txnrd2*-deficient tumors also expressed significantly higher levels of grx2 than WT tumors ( $n = 3$  tumors per group, Supplementary Fig. 1A; Supplementary Data are available online at [www.liebertpub.com/ars](http://www.liebertpub.com/ars)). Subsequently, BSO was administered *via* the drinking water, which proved highly efficient. Glutathione levels dropped sharply, as shown by high-performance liquid chromatography (HPLC) analysis (Fig. 3A). Reduced glutathione (GSH) ( $0.0007 \pm 0.0002 \mu\text{mol}/\mu\text{g}$  protein) and oxidized glutathione (GSSG) levels ( $0.0008 \pm 0.0003 \mu\text{mol}/\mu\text{g}$  protein) were considerably diminished in *Txnrd2*-deficient tumors compared with untreated *Txnrd2*<sup>-/-</sup> tumors when BSO was administered *via* the drinking water (GSH  $0.015 \pm 0.003$ ; GSSG  $0.003 \pm 0.001 \mu\text{mol}/\mu\text{g}$  protein) ( $n = 8$  tumors per group, Fig. 3A, B). The decrease of the GSH/GSSG ratio in BSO-treated *Txnrd2* null tumors indicates elevated levels of oxidative stress (Fig. 3C,  $n = 8$  tumors per group). Most importantly, manipulation of *in vivo* glutathione levels by BSO caused a further reduction of *Txnrd2*-deficient tumor mass by  $\sim 38\%$  ( $0.52 \pm 0.14$  g) compared with untreated *Txnrd2*<sup>-/-</sup> tumors ( $0.84 \pm 0.27$  g,  $n = 8$ , Fig. 3D).

#### Loss of *Txnrd2* delays the angiogenic switch and impairs tumor angiogenesis

The tumor-surrounding vascular network of *Txnrd2*-deficient tumors was less prominent compared with WT tumors (Fig. 4A). In line, quantification of tumor vessels

demonstrated significantly fewer vessels per *Txnrd2*-deficient tumor ( $143 \pm 13.9$ ) compared with WT tumors ( $239 \pm 30.43$ ,  $n = 6$ , Fig. 4B).

#### Reduced expression of key angiogenic players in tumors derived from *Txnrd2*<sup>-/-</sup> cells

The delayed angiogenic switch and the diminished vascularization could be attributed to a substantial reduction of Hif-1 $\alpha$  protein levels in *Txnrd2*-deficient tumors (day 3:  $38\% \pm 2\%$ ; day 6:  $41\% \pm 7\%$ ) compared with tumors expressing *Txnrd2* (day 3, day 6: arbitrarily set to 100%) at both time points ( $n = 4$  per time point, Fig. 4C). In accordance, vascular endothelial growth factor A (VEGF-A) levels were also significantly reduced at day 3 ( $18\% \pm 2\%$ ) in these tumors compared with *Txnrd2* WT tumors (arbitrarily set to 100%, Fig. 4C). This phenotype was still present on day 6 of tumor growth (*Txnrd2*<sup>+/+</sup>: arbitrarily set to 100% vs. *Txnrd2*<sup>-/-</sup>:  $59\% \pm 2\%$ ). An ELISA specific for mouse VEGF confirmed that *Txnrd2*-deficient tumors contained less VEGF-A ( $n = 4$  per time point, day 3:  $0.19 \pm 0.06 \text{ pg}/\mu\text{g}$  protein; day 6:  $0.09 \pm 0.05 \text{ pg}/\mu\text{g}$  protein) than WT tumors (day 3:  $0.48 \pm 0.24 \text{ pg}/\mu\text{g}$  protein day 6:  $0.12 \pm 0.05 \text{ pg}/\mu\text{g}$  protein) (data not shown).

#### Hif-1 $\alpha$ stabilization in response to serum withdrawal and hypoxia is impaired

Under normal cell culture conditions, Hif-1 $\alpha$  expression was barely detectable in either cell line (*Txnrd2*<sup>+/+</sup>: arbitrarily

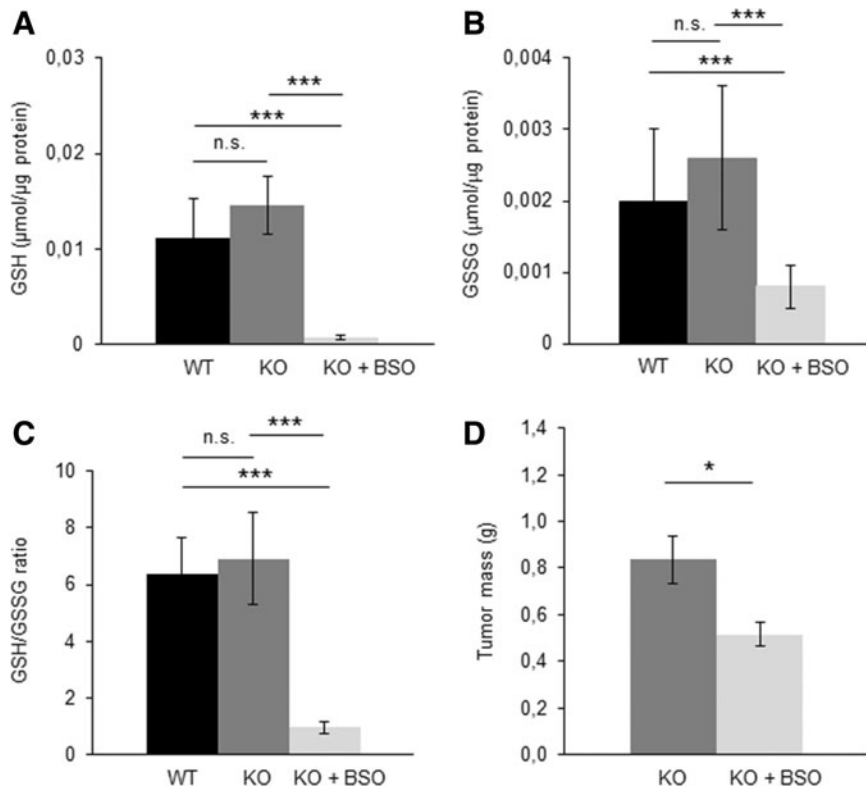


**FIG. 3. Loss of *Txnrd2* renders tumors susceptible to GSH depletion.** (A) Pharmacological glutathione depletion by BSO was confirmed by HPLC in tumor samples. (B) BSO treatment efficiently depleted tumors from glutathione as determined by measuring the levels of GSSG by HPLC. (C) The decrease of the GSH/GSSG ratio in BSO-treated *Txnrd2* null tumors indicates elevated levels of oxidative stress. (D) BSO treatment of tumor-bearing mice *via* the drinking water caused a further reduction in growth of *Txnrd2* null tumors. Data in (A, B) are represented as mean  $\pm$  SD, data in (C, D) as mean  $\pm$  SEM. \* $p$  < 0.05, \*\*\* $p$  < 0.001. BSO, L-buthionine sulfoximine.

set to 100% vs. *Txnrd2*<sup>-/-</sup>: 50%  $\pm$  16.7%,  $n$  = 6, Fig. 4D). However, Hif-1 $\alpha$  expression substantially increased in WT cells but not in *Txnrd2*-deficient cells after serum withdrawal (*Txnrd2*<sup>+/+</sup>: 4830%  $\pm$  2640% vs. *Txnrd2*<sup>-/-</sup>: 70%  $\pm$  17.3%) ( $n$  = 6, Fig. 4D). A similar effect was also observed under hypoxic conditions ( $n$  = 4, Supplementary Fig. S1C).

To investigate whether Hif-1 $\alpha$  is regulated at the transcriptional and/or the translational level, *Hif-1 $\alpha$*  mRNA expression levels were assessed by quantitative real-time-polymerase chain reaction (qRT-PCR). Under normal cell culture conditions, *Hif-1 $\alpha$*  mRNA levels were comparable (*Txnrd2*<sup>+/+</sup>: arbitrarily set to 100% vs. *Txnrd2*<sup>-/-</sup>: 110%  $\pm$  26%,  $n$  = 5, data not shown). Starvation resulted in a moderate increase in WT cells, whereas *Txnrd2*-deficient cells failed to upregulate *Hif-1 $\alpha$*  mRNA levels (*Txnrd2*<sup>+/+</sup>: 190%  $\pm$  78% vs. *Txnrd2*<sup>-/-</sup>: 90%  $\pm$  35%). These data indicate that stabilization of the majority of Hif-1 $\alpha$  occurs at the protein level since the small change of *Hif-1 $\alpha$*  transcripts was unlikely to account for the increased levels of Hif-1 $\alpha$  protein in WT cells.

#### Increased PHD2 expression promotes Hif-1 $\alpha$ protein degradation in *Txnrd2*<sup>-/-</sup> cells and tumors

Next, we examined some upstream regulators of Hif-1 $\alpha$  protein stability, including HIF prolyl hydroxylases. Interestingly, even under baseline conditions, PHD2 protein levels were elevated in *Txnrd2*<sup>-/-</sup> cells compared with control cells (*Txnrd2*<sup>+/+</sup>: arbitrarily set to 100% vs. *Txnrd2*<sup>-/-</sup>: 322.2%  $\pm$  99.8%,  $n$  = 4, Fig. 5A). Vice versa, knockdown of PHD2 using siRNA increased Hif-1 $\alpha$  protein levels in both WT and *Txnrd2*-deficient MEFs, thereby substantiating that PHD2 is the main regulator of Hif-1 $\alpha$  protein stability ( $n$  = 3, Supplementary Fig. S1D).

Serum starvation had no additional impact on PHD2 protein expression in either of the cell lines ( $n$  = 4, Fig. 5A). Consistent with these *in vitro* findings, *Txnrd2* null tumors also displayed augmented PHD2 expression ( $n$  = 3, Supplementary Fig. S1B).

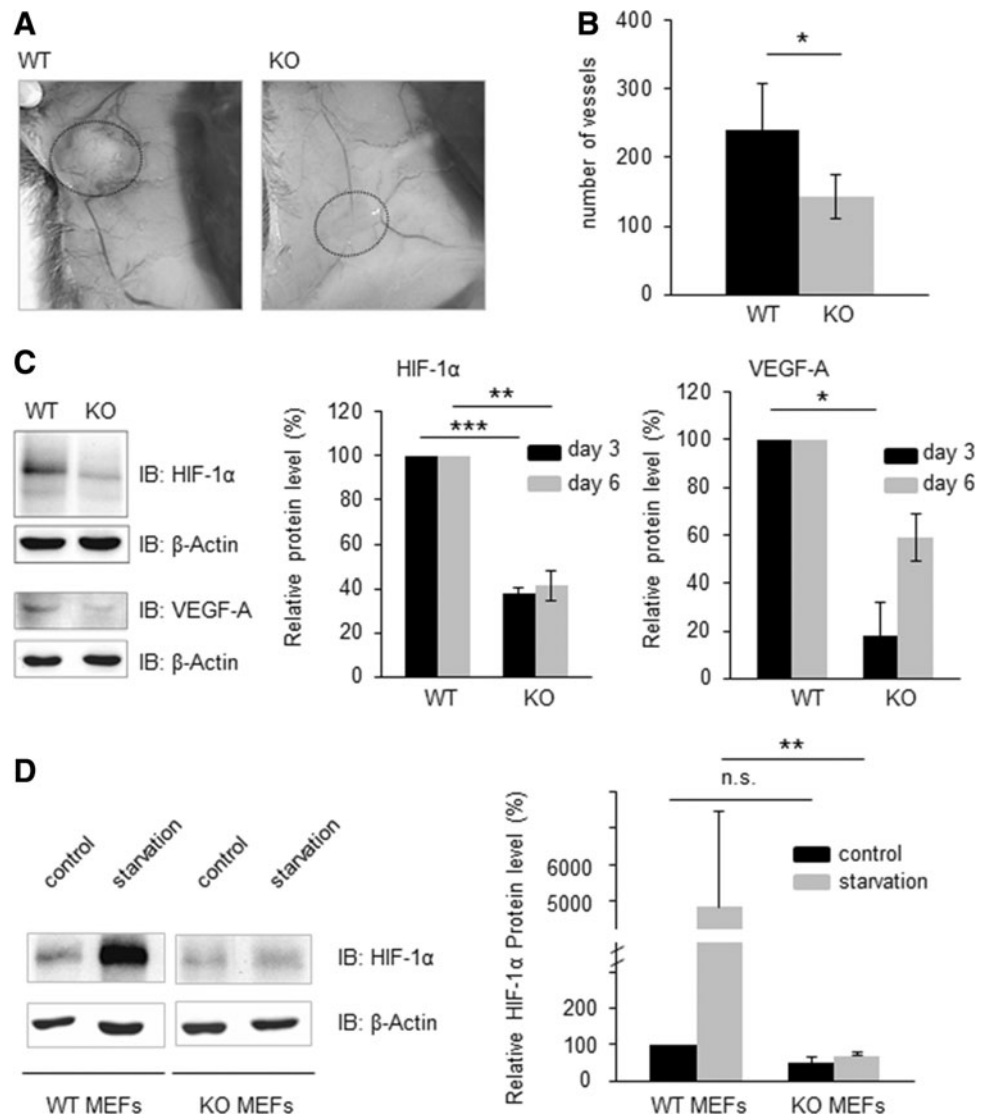
To examine whether the mRNA levels were also increased, we performed qRT-PCR. Indeed, *Txnrd2*<sup>-/-</sup> cells showed statistically significant enhanced levels of *PHD2* mRNA ( $n$  = 11, WT arbitrarily set to 100% vs. KO 242%  $\pm$  55%, data not shown).

Apart from affecting Hif-1 $\alpha$  stabilization, PHD2 is also a well-known regulator of nuclear factor- $\kappa$ B (NF- $\kappa$ B) activity (11). Indeed, immunocytochemistry revealed reduced nuclear translocation of the p65 NF- $\kappa$ B subunit in *Txnrd2* null cells (Fig. 5B). Quantification of nuclear translocation of p65 confirmed this observation ( $n$  = 6, Fig. 5C).

#### Enhanced JNK phosphorylation leads to increased PHD2 protein levels

Intrigued by the findings that *Txnrd2* deletion impairs tumor growth *via* an increase in PHD2 expression, we endeavored to unmask a previously unknown link between *Txnrd2* and PHD2. Since JNK is known to be regulated by the cellular redox status (27), we investigated its phosphorylation status. Indeed, JNK phosphorylation was increased in immortalized *Txnrd2*<sup>-/-</sup> cells in contrast to their WT counterparts ( $n$  = 5, Fig. 6A) and this effect could be attributed to elevated ROS as the phosphorylation status could be reduced by addition of polyethylene glycol-conjugated catalase (PEG-catalase) ( $n$  = 4, Fig. 6B). Substantiating our hypothesis that ROS-induced, sustained JNK activation leads to elevated PHD2 expression, PEG-catalase treatment also

**FIG. 4. Loss of *Txnrd2* delays the angiogenic switch and reduces tumor vascularization. (A)** The tumor-surrounding vascular network was less prominent in the *Txnrd2* null tumors at 3 days after tumor inoculation. Dotted circles outline the tumor tissue. **(B)** Quantification of the vessels by CD31 staining confirmed the morphological finding illustrated in (A). **(C)** Analysis of key-angiogenic factors revealed decreased Hif-1 $\alpha$  as well as VEGF-A protein expression in *Txnrd2* null tumor tissues at days 3 and 6 of tumor growth. \* $p < 0.05$ , \*\* $p < 0.01$ , \*\*\* $p < 0.001$ . *Left panel*: representative immunoblots from day 3; *middle and right panels*: semi-quantitative assessment of immunoblots. **(D)** Transformed *Txnrd2*<sup>-/-</sup> cells failed to stabilize Hif-1 $\alpha$  protein after serum starvation. *Left panel*: representative immunoblot; *right panel*: semi-quantitative assessment of immunoblots. All data are represented as mean  $\pm$  SD. Hif-1 $\alpha$ , hypoxia-inducible factor-1 $\alpha$ ; VEGF-A, vascular endothelial growth factor A.



blunted PHD2 expression ( $n=4$ , Fig. 6B). To provide a molecular link between mitochondrial ROS and increased JNK-phosphorylation, we measured PTP activity. ROS have been implicated in this pathway through inhibition of the counteracting JNK phosphatases (27), and measurements of protein tyrosine phosphatase (PTP) activity, indeed, demonstrated a reduced activity in the *Txnrd2*-deficient cells ( $n=7$ , Fig. 6F).

To investigate whether the *Txnrd2*-dependent PHD2 regulation was a general mechanism and not a cell type-specific effect, we manipulated *Txnrd2* expression levels in the murine lung tumor cell line LLC1. Using endoribonuclease-prepared small interfering RNA (esiRNA), we were able to decrease *Txnrd2* protein levels by  $\sim 90\%$  compared with scrambled esiRNA-treated cells ( $n=4$ , Fig. 6C). This knockdown led to a subsequent increase in pJNK and PHD2 levels in *Txnrd2*-deficient LLC1 cells. Furthermore, treating *Txnrd2* KO MEFs and LLC1 cells with the JNK inhibitor SP600125 caused both a decrease of basal pJNK levels and a strong decrease in PHD2 expression, which is in accordance with the proposed mechanism ( $n=5$ , Fig. 6D). These data demonstrate that

this *Txnrd2*-pJNK-PHD2 axis is also a relevant pathway for bona fide tumor cells. Finally, knockdown of JNK by siRNA significantly attenuated PHD2 expression (control siRNA arbitrarily set to 100%, siRNA: JNK  $22.6\% \pm 3.7\%$ , PHD2  $53.2\% \pm 6.3\%$ ,  $n=13$ , exemplarily shown in Fig. 6E), further substantiating our findings that JNK acts as an upstream participant in this pathway.

#### Expression of *Txnrd2* in human cancer tissue

To demonstrate that our findings are also of relevance for human tumors, the expression of *Txnrd2* was studied by immunohistochemistry in human cancer tissue derived from three different types of tumors: colon carcinoma ( $n=10$ ), hepatocellular carcinoma ( $n=8$ ), as well as lung adenocarcinoma ( $n=8$ ). In colon carcinomas as well as in hepatocellular carcinomas, we could observe an abundant expression of *Txnrd2*. Lung adenocarcinomas also expressed *Txnrd2*, however to a much lesser extent than in the colon and liver samples (Supplementary Fig. S2). These observations are in line with previously published reports (9, 49) as well as with the human protein atlas (48).

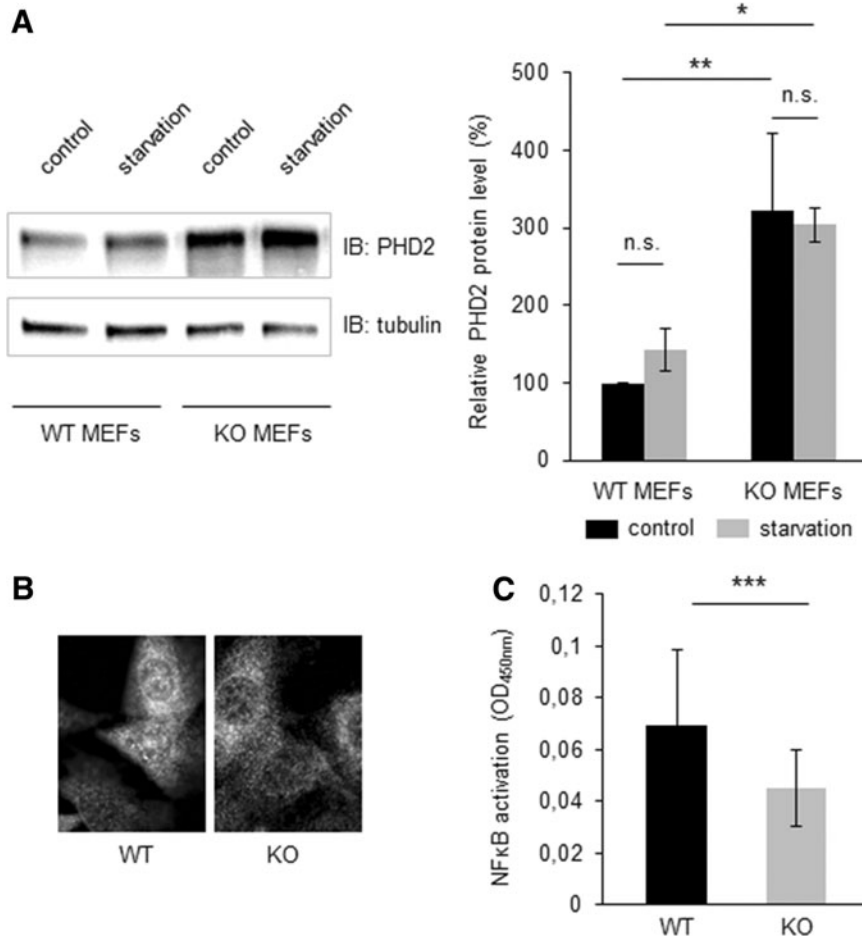


**FIG. 5. PHD2 protein levels are highly increased in *Txnrd2* null cells.** (A) PHD2 protein levels are strongly increased in *Txnrd2*<sup>-/-</sup> cells, both under normal cell culture conditions and in response to starvation. Data are represented as mean ± SEM. (B) Nuclear translocation of the p65 subunit of NFκB is diminished in *Txnrd2*<sup>-/-</sup> cells as shown by immunocytochemistry. (C) An NFκB-specific transcription factor assay confirmed the data shown in (B). \**p* < 0.05, \*\**p* < 0.01, \*\*\**p* < 0.001. Data are represented as mean ± SD.

## Discussion

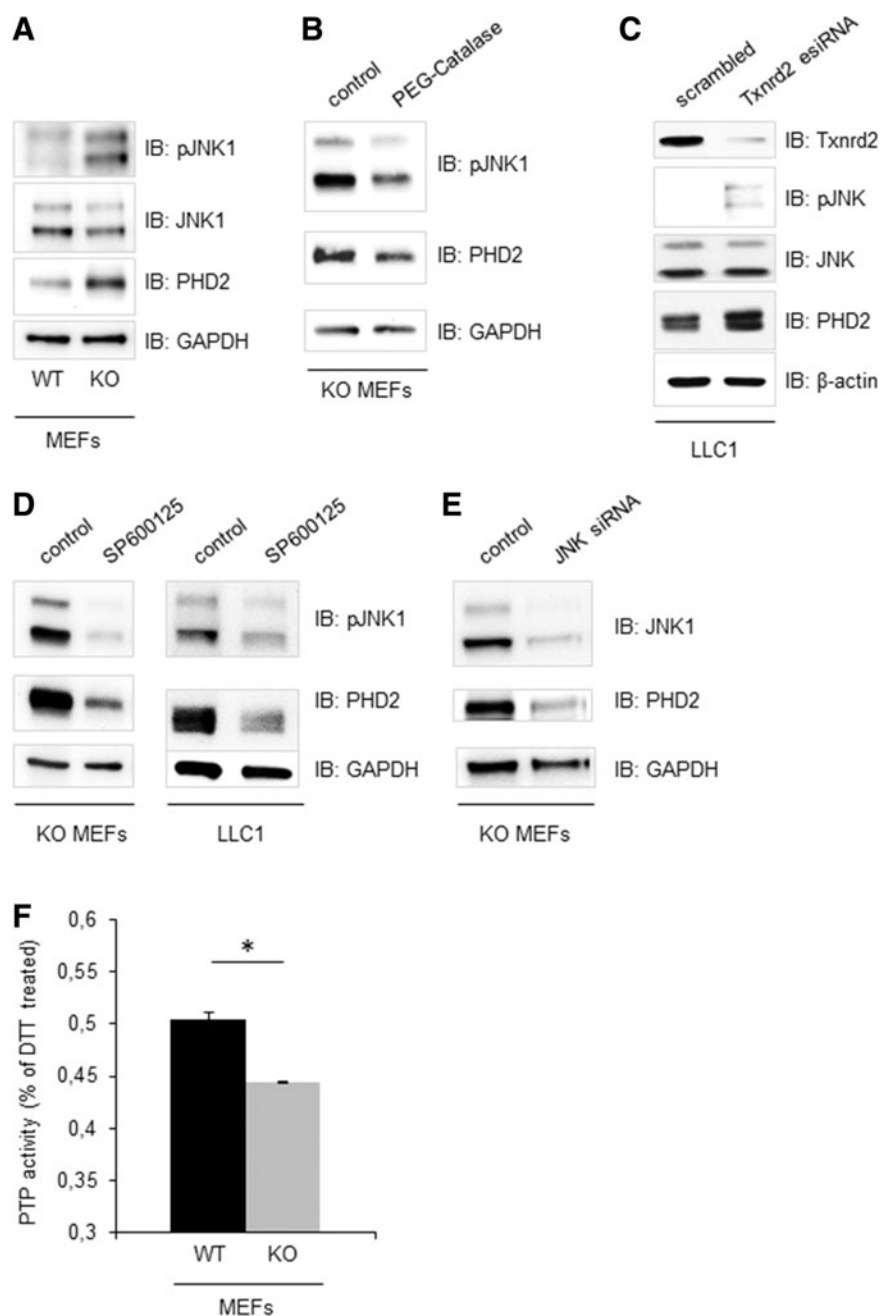
Elevated levels of ROS have been detected in almost all cancers, where they promote many aspects of tumor development and progression, including DNA damage, activation of inflammatory pathways, receptor tyrosine kinase signaling, and stabilization of Hif-1α (30). On the other hand, several oncogenes were recently discovered to act as active inducers of NF-E2-related factor-2 (*Nrf2*), which, in turn, promotes an ROS detoxification program required for tumor initiation (13). Moreover, most tumor cells also express increased levels of antioxidants to detoxify ROS, suggesting that a delicately balanced elevation of intracellular ROS levels is required for cancer cell function (30, 40).

Since the PrxIII-Trx2-Txnrd2 node is considered the most important route for mitochondrial H<sub>2</sub>O<sub>2</sub> removal (14, 45) and we observed an abundant expression of Txnrd2 in a variety of human tumors (Supplementary Fig. S2), we employed genetically engineered Txnrd2-deficient cells to study the effects of an altered mitochondrial redox balance on tumor signaling and growth. Indeed, our model enabled us to unveil how a chronic change of this balance affects Hif signaling and tumor growth *via* a previously unknown pathway. The cornerstones of this pathway encompass a ROS-dependent activation of JNK after the loss of *Txnrd2*, elevated PHD2 protein and mRNA expression, a failure to stabilize Hif-1α in response to hypoxia and other stressors, and decreased VEGF-A levels. *In vivo* we could observe a delayed angio-

genic switch, attenuated tumor vascularization, and, ultimately, reduced growth of tumors lacking *Txnrd2*.

Unexpectedly and in contrast to previous results (5, 8, 17), loss of *Txnrd2* followed by a compensatory increase in *grx2* expression, as well as moderately increased ROS levels, did not stabilize Hif-1α. Numerous studies have demonstrated that addition of exogenous ROS leads to the stabilization of Hif-1α protein and activation of Hif target genes such as VEGF-A (4, 8, 15). In accordance, tumor cell-derived ROS can regulate angiogenesis and tumor growth through VEGF (52) and exposure to antioxidants has been demonstrated to delay tumorigenesis by reducing HIF levels (16). Given the previous reports, we expected that the *Txnrd2* deletion and coincident further elevation of ROS levels would lead to a stabilization of the Hif-1α protein through PHD2 inactivation; for instance, by oxidizing PHD-bound Fe(II) to Fe(III) (17, 38), and/or the cysteine residue 201 within the catalytic domain of PHD2, thereby further inhibiting PHD2 activity (35, 37). In this study, we observed quite the contrary: Hif-1α protein levels were reduced not only in *Txnrd2*<sup>-/-</sup> tumors but also in *Txnrd2*<sup>-/-</sup> MEFs, particularly following certain stressors such as hypoxia or serum starvation. The diminished Hif-1α levels could be attributed to high PHD2 expression, which leads to hydroxylation of key proline residues of Hif-1α and subsequent targeting of Hif-1α to the proteasome (25, 26). Considering the existing reports in the literature, these findings indicate that, apparently, PHD2 is differentially regulated upon a ROS challenge. In contrast to an acute and

**FIG. 6. Deletion of *Txnrd2* increases PHD2 expression via sustained JNK phosphorylation.** (A) Representative immunoblot showing the substantially augmented presence of phosphorylated JNK (pJNK) in *Txnrd2* null MEFs. (B) PEG-catalase treatment of *Txnrd2*<sup>-/-</sup> cells not only lowered the phosphorylation of JNK but also reduced the overall PHD2 protein levels. (C) Knockdown of *Txnrd2* in the bona fide tumor cell line LLC1 led to a subsequent increase of PHD2 and pJNK protein levels. (D) The JNK inhibitor SP600125 reduced phosphorylated JNK as well as PHD2 protein levels in both transformed *Txnrd2*<sup>-/-</sup> cells and the *Txnrd2*-deficient tumor cell line, LLC1. (E) siRNA-mediated knockdown of JNK in *Txnrd2*<sup>-/-</sup> MEFs also led to a reduction in PHD2 expression levels. (F) PTP-activity is significantly reduced in *Txnrd2*<sup>-/-</sup> cells compared with WT cells. \**p* < 0.05. JNK, c-Jun NH2-terminal Kinase; MEFs, mouse embryonic fibroblasts; PEG-catalase, polyethylene glycol-conjugated catalase; PTP, protein tyrosine phosphatase.



possibly nonphysiological, exogenous bolus administration of ROS that inhibits PHD2 activity, a compensatory expression of the mitochondria-located oxidoreductase *grx2* is induced in *Txnrd2*-deficient cells, thereby keeping the emission of ROS from the mitochondria in a cell-tolerable, however moderately elevated range. This continuous and modest elevation of endogenous ROS in *Txnrd2*-deficient cells appears to result in an adaptive upregulation of PHD2 protein levels, possibly as a protective measure against chronically increased Hif-1 $\alpha$  expression. A similar adaptive mechanism has also been observed during chronic hypoxia. Acute hypoxia impairs PHD2 activity, whereas chronic hypoxia inhibits mitochondrial respiration, thus restoring oxygen availability and leading to PHD2 overactivation (18).

In pursuit of a molecular link between mitochondrial ROS and increased PHD2 expression, we investigated the redox-sensitive JNK signaling pathway. ROS-induced JNK phosphorylation *via* Mitogen-activated protein kinase kinase 4 (MKK4) can be initiated by the liberation of the apoptosis signal-regulating kinase 1 (ASK-1) from its endogenous suppressor, reduced thioredoxin 1 (42). Furthermore, ROS have been implicated in this pathway through inhibition of JNK phosphatases (27) and we could indeed measure a reduced activity of PTPs in the *Txnrd2*-deficient cells. Furthermore, we could show that JNK phosphorylation was markedly increased in *Txnrd2*<sup>-/-</sup> cells as well as in the established mouse cancer cell line, LLC1, when *Txnrd2* was knocked down. Administration of the JNK inhibitor SP600125 and knockdown of JNK by siRNA substantiated



our hypothesized mechanism, as this led to reduced PHD2 protein levels, thus confirming the yet-unrecognized link between JNK and PHD2 expression. Currently, it remains to be shown how exactly PHD2 levels are regulated by activated JNK.

Taken together, our *in vitro* observations serve as a plausible foundation for the restricted growth of *Txnrd2*-null tumors. First, JNK signaling has been shown to suppress tumor growth (33, 50). Second, tumor angiogenesis is, at least partly, regulated by PHD2 (7), and *Txnrd2*-null tumors express reduced Hif-1 $\alpha$  as well as reduced VEGF-A protein levels. Finally, PHD2 has additional Hif-independent tumor suppressor functions (7), which are also in agreement with the reduced tumor growth observed in our model.

We previously showed that primary *Txnrd2*<sup>-/-</sup> fibroblasts are highly sensitive to GSH depletion-induced cell death (10). As demonstrated here, this apparently also holds true for immortalized cells and tumors derived thereof, most likely due to a block of the compensatory GSH-dependent Prx III reduction by grx2. For future studies targeting antioxidants to efficiently combat cancer, we therefore suggest the concomitant targeting of at least two key antioxidant systems.

In conclusion, our data describe a hitherto unrecognized pathway for PHD2 activation *via* JNK, originating from an altered mitochondrial redox balance. Phosphorylated JNK leads to a sustained expression of PHD2 in a yet unknown manner, ultimately leading to the impairment of Hif-1 $\alpha$  signaling. While our data oppose previous results on PHD2 inhibition by ROS, this should be rationalized on the basis of variations in the models regarding radicals, sources of ROS, as well as their concentrations and the duration in which they are present.

Although our study only scratches the surface regarding the relevance of *Txnrd2* for human cancer biology, we hope it will motivate other groups to study ROS-controlling systems in this context. Finally, our findings highlight the need for future anti-cancer strategies to consider the fine tuning of intracellular ROS signaling to efficiently shift cells from ROS-dependent tumor growth-promoting events toward ROS-induced cell death signaling.

## Materials and Methods

### Cell lines and reagents

*Txnrd2*<sup>+/+</sup> and *Txnrd2*<sup>-/-</sup> MEFs were isolated from embryos at embryonic day E12.5 from breeding of heterozygous *Txnrd2* mice. Genotyping and cell culturing was performed as previously described (10). Primer sequences are listed in Supplementary Tables S1 and S2. Primary MEFs (passage number <10) were immortalized by serial passaging (passage number >10) as described (39). LLC1 cells were obtained from ATCC (Teddington, United Kingdom). To induce Hif-1 $\alpha$  protein expression, cells were either cultured in serum-free medium for 4 h or kept in a hypoxic chamber (1% O<sub>2</sub>) for 6 h.

### Generation of transformed *Txnrd2*<sup>+/+</sup> and *Txnrd2*<sup>-/-</sup> cells

For the transformation of cells, MEFs were co-transduced with c-Myc and Ha-ras<sup>V12</sup>-expressing lentiviruses as described (31). Soft agarose assays were performed to select

successfully transformed cells. After 7 days of growth in soft agarose, single-cell-derived colonies were isolated, expanded, and analyzed for expression of *Txnrd2*, c-Myc, and Ha-ras<sup>V12</sup>. To assess the efficacy of transformation with c-Myc and Ha-ras<sup>V12</sup>, cells were analyzed for green fluorescent protein (GFP) expression using BD FACSort (Beckton Dickinson, Heidelberg, Germany). Data were analyzed using the CellQuest software (Beckton Dickinson) and WinMDI software, version 2.9 (Scripps Research Institute, La Jolla, CA).

### Proliferation assay

Cell proliferation and cytotoxicity were measured using the electronic cell sensor array technology xCELLigence (Roche, Mannheim, Germany) as described (32). BSO (Sigma-Aldrich, Munich, Germany) was used at a final concentration of 10  $\mu$ M to inhibit the *de novo* synthesis of GSH.

### Measurement of cellular ROS levels

ROS generation was assessed using CellROX Deep Red Reagent (Life Technologies, Darmstadt, Germany) according to the manufacturer's recommendations. Fluorescence intensity was analyzed by flow cytometry using a Gallios 2/8 flow cytometer (Becton Coulter, Krefeld, Germany) at an excitation wavelength of 633 nm and emission collected with a 660 band-pass detector. Cells were gated and analyzed using the Gallios Data acquisition and analysis software (Becton Coulter).

### Measurement of GSH concentration in cells and tumors

Total glutathione content in cells was analyzed by performing a modified assay based on a method first described by Tietze (46). The concentration of total glutathione in cells was calculated as  $\mu$ M/mg protein and referenced to a 10 mM GSH calibration solution (Sigma-Aldrich). Reduced and oxidized glutathione concentrations (GSH and GSSG) in tumor samples were measured by isocratic HPLC as previously described (31).

### Quantitative real-time PCR

The expression of *Hif-1 $\alpha$* , *PHD2*, and *Txnrd2* was investigated by RT-PCR/qRT-PCR as described (31). Expression was normalized to  $\beta$ -actin or *aldolase* expression. Primer sequences are listed in Supplementary Table S2.

### Hematoxylin-eosin staining/immunohistochemistry/immunofluorescence and image analysis

Paraformaldehyde-fixed (4% w/v, in phosphate-buffered solution [PBS]) and paraffin-embedded tumor material was cut in 5  $\mu$ m-thick sections and stained as described (10). Hematoxylin-eosin (H&E) staining, immunohistochemistry, and immunofluorescence staining were performed as previously described (2). Antibodies are listed in Supplementary Table S3. As control, primary antibodies were omitted during staining. Slides for peroxidase staining were incubated with peroxidase-conjugated streptavidin (Vectastain KIT ABC; Vector Laboratories, Linaris, Wertheim-Bettingen, Germany). Thereafter, slides were incubated with Vector<sup>®</sup> DAB

kit or AEC kit (Vector Laboratories). Sections were counterstained with hematoxylin. Sections for immunofluorescence were counterstained with 4,6-diamidino-2-phenylindole ([DAPI], Hard Set™ Mounting Medium; Vector Laboratories). Immunostaining was analyzed using the Olympus BX41 microscope in combination with the CAMEDIA C-5050 digital camera and the software Olympus DP-Soft v3.2 (Olympus, Tokyo, Japan). For the quantification of tumor vascularization, tumor cell proliferation, tumor cell apoptosis, and necrosis, three representative sections per tumor were analyzed ( $n=6$  tumors) and micrographs were obtained from five random regions of interest from all three sections. Altogether, the analysis of these 15 random microscopic visual fields per tumor was performed in a blinded fashion by two researchers using a 20× objective. Total blood vessels were determined by counting the number of CD31-positive blood vessels. Proliferation was studied by counting Ki-67 positive and -negative cells. The ratio of proliferative to nonproliferative cells was expressed as PI. Apoptosis was assessed by counting caspase-3 positive cells. For the determination of necrosis, the percentage of the necrotic area relative to the entire tumor area was measured on H&E stained tumor sections.

#### Immunoblotting

Immunoblotting was performed as previously described (1). Primary antibodies are listed in Supplementary Table S4. Detection of *Txnrd2* expression was achieved with a *Txnrd2*-specific antibody as described (31). Nuclear translocation of Hif-1 $\alpha$  in cells was analyzed with the NE-PER® Nuclear and Cytoplasmic Extraction Reagent (Fisher Scientific GmbH, Schwerte, Germany). Equal loading was confirmed with a lamin-specific antibody. To block H<sub>2</sub>O<sub>2</sub>, cells were treated with PEG-catalase (50 U/ml; Sigma-Aldrich) for 18 h.

To analyze the levels of phosphorylated JNK, samples were lysed with buffer containing sodium fluoride (0.5 mM) and Na<sub>3</sub>VO<sub>4</sub> (0.5 mM) (Sigma Aldrich). All blots were stripped and reprobed with either  $\beta$ -actin or glyceraldehyde 3-phosphate dehydrogenase (GAPDH). To block JNK activation, the specific JNK-inhibitor SP600125 (#420119, 50  $\mu$ M; Merck Millipore, Schwalbach, Germany) was applied to the cell culture medium, either for 8 h or overnight. Application of dimethyl sulfoxide (DMSO) served as a control.

#### PHD2 knockdown in *Txnrd2*<sup>+/+</sup> and *Txnrd2*<sup>-/-</sup> MEFs

MEFs were transfected with siMax siRNA (Eurofins Genomics, Ebersberg, Germany) using the following sequences: *PHD2* siRNA 5'-GUG GAG GUA UUC UUC GAA UTT-3'; scramble siRNA 5'-UUC UUC GAA CGU GUC ACG UTT-3'. 10<sup>5</sup> cells were seeded onto 12-well plates and incubated with 5 nM siRNA and HiPerfect transfection reagent (Qiagen, Hilden, Germany) in full medium for 50 h. Subsequently, cells were washed in PBS and proteins were extracted by cell lysis. Knockdown of PHD2 was confirmed by immunoblot.

#### *Txnrd2* knockdown in LLC1 tumor cells

LLC1 cells were transfected with MISSION® esiRNA targeting mouse *Txnrd2* (EMU067221; Sigma-Aldrich) according to the manufacturer's instructions. Cells were harvested, lysed for 72 h after transfection, and blotted against designated antibodies as described earlier.

#### JNK knockdown in *Txnrd2*<sup>-/-</sup> MEFs

MEFs were transfected with FlexiTube siRNA (Qiagen) against both *JNK1* (GS26419) and *JNK2* (GS26420). Reverse transfection was performed in 24-well plates according to the manufacturer's advice using 5  $\mu$ l HiPerFect transfection reagent and 50 nM siRNA for 70,000 cells for 72 h. Subsequently, cells were lysed and knockdown of JNK was confirmed by immunoblot.

#### Enzyme-linked immunosorbent assay

To measure mouse VEGF in cell culture supernatants and tumor tissue, the Mouse VEGF Quantikine Immunoassay (R&D Systems, Wiesbaden-Nordenstedt, Germany) was employed according to the manufacturer's recommendations. Absorbance was measured at a wavelength of 450 nm using the ELISA plate reader Infinite F200 (Tecan, Crailsheim, Germany). Total protein concentration in supernatants and tumor homogenates was measured with the BCA™ Protein Assay Kit (Pierce; Fisher Scientific).

#### Subcutaneous xenograft tumor model

Transformed *Txnrd2*<sup>-/-</sup> and *Txnrd2*<sup>+/+</sup> cells ( $4 \times 10^6$  cells dissolved in 200  $\mu$ l sterile PBS) were injected subcutaneously into the retral flank of C57BL/6 mice. Tumors were collected over a period of 11 days. All animal experiments were performed in compliance with the German Animal Welfare Law and had been approved by the institutional committee on animal experimentation and the government of Upper Bavaria.

#### Treatment of tumor-bearing mice with BSO

For the *in vivo* pharmacological studies,  $4 \times 10^6$  transformed *Txnrd2*-deficient cells in 200  $\mu$ l sterile PBS were injected subcutaneously into the retral flank of C57BL/6 mice. Tumors were allowed to settle for 3 days. From day 3 onward, BSO (20 mM) was administered *via* the drinking water for 8 days. BSO-containing water was exchanged every third day. At day 11, mice were sacrificed and tumor mass and volume was analyzed.

#### Measurement of PTP activity

PTP activity in total cell lysates was measured toward a <sup>32</sup>P-labeled phosphotyrosine substrate (AEEEI<sub>p</sub>YGEFEA KKKK) as previously described (43). WT and *Txnrd2*<sup>-/-</sup> fibroblasts were starved overnight in phenol-red free DMEM (Gibco, Stockholm, Sweden) with 1% fetal calf serum. Cells were washed in 20 mM Hepes pH 7.4 (Sigma-Aldrich, Stockholm, Sweden) and lysed in degassed lysis buffer (50 mM sodium acetate, 150 mM NaCl, 1% NP-40, 25  $\mu$ g/ml aprotinin, 25  $\mu$ g/ml leupeptin, 250 U/ml catalase, and 125 U/ml superoxide dismutase [Calbiochem, Solna, Sweden]). Lysates were cleared by centrifugation at 21,000 g at 4°C for 5 min. A fraction of the lysate was mixed with deoxygenated 25 mM imidazole pH 7.4 (Sigma-Aldrich), the PTP substrate (kind gift from Carl Henrik Heldin) was added, and the mixture was incubated for 20 min. The dephosphorylation reaction was stopped by addition of a charcoal mixture (0.9M HCl, 90 mM sodium pyrophosphate, 2 mM NaH<sub>2</sub>PO<sub>4</sub>, 4% vol/vol NoritA; Sigma-Aldrich) and centrifuged at 21,000 g for 3 min. The supernatant containing released <sup>32</sup>P (PerkinElmer, Upplands Väsby, Sweden) was transferred to scintillation vials (Sigma-

Aldrich) with EcoScint A (National Diagnostics, BioNordika, Stockholm, Sweden), and radioactivity was measured using a Wallac Winspectral 1414 Liquid Scintillation Counter (PerkinElmer). The radioactive signal reflects the activity of the reduced PTPs and was normalized toward cell lysate treated with the reducing agent dithiothreitol (DTT; Sigma-Aldrich) that represents the maximal activity when all PTPs are reduced.

#### Determination of NF $\kappa$ B activation

Translocation of the NF $\kappa$ B subunit p65 to the nucleus was analyzed by immunocytochemistry in formaldehyde-fixed MEFs as described (3). In brief, cells were grown to ~80% confluence on glass coverslips coated with collagen G (10  $\mu$ g/ml; Biochrom AG, Berlin, Germany). Subsequently, cells were fixed with 3.7% formaldehyde, permeabilized with 0.3% Triton X-100, and incubated with a p65-specific antibody. Slides were mounted with DAPI-containing Hard Set Mounting Medium (Vector Laboratories) and analyzed using the confocal laser scanning microscope Leica TCS SP5 (Leica Microsystems, Wetzlar, Germany).

To further substantiate the results from immunocytochemistry, activation of the NF $\kappa$ B subunit p65 was measured using the colorimetric NF $\kappa$ B p65 EZ-TFA transcription factor assay according to the manufacturer's instructions (Millipore GmbH, Schwalbach, Germany).

#### Statistical analysis

Statistical analysis was performed using SigmaPlot<sup>®</sup> 11.0 software (Jandel GmbH, Erkrath, Germany). Experimental values are expressed as mean  $\pm$  standard deviation, unless stated otherwise. Numbers of independent experiments are indicated in the corresponding results section. Statistically significant differences between groups were calculated by Student's *t*-test or analysis of variance followed by Bonferroni's correction. Non-Gaussian distributed data were analyzed by the nonparametric Kruskal–Wallis test for nonpaired data. *p* < 0.05 was considered significant.

#### Acknowledgments

The authors thank Dora Kiesl, Dorothee Gössel, Heidi Förster, Kasia Stefanowski, and Matthias Semisch for their excellent technical assistance.

This work was supported by the Deutsche Forschungsgemeinschaft (DFG) priority Program SPP 1190 to H.B. and M.C., the Friedrich-Baur Stiftung to H.B. and T.F., a DFG grant (CO 291/2-3) to M.C., a Marie Curie Actions Fellowship of the FP7 People Program to J.K., and a fellowship from Alexander von Humboldt-Stiftung to J.P.F.A.

#### Author Disclosure Statement

No competing financial interests exist.

#### References

- Arner ES and Holmgren A. The thioredoxin system in cancer-introduction to a thematic volume of Seminars in Cancer Biology. *Semin Cancer Biol* 16: 419, 2006.
- Beck H, Acker T, Wiessner C, Allegrini PR, and Plate KH. Expression of angiopoietin-1, angiopoietin-2, and tie receptors after middle cerebral artery occlusion in the rat. *Am J Pathol* 157: 1473–1483, 2000.
- Belaiba RS, Bonello S, Zahringer C, Schmidt S, Hess J, Kietzmann T, and Gorchach A. Hypoxia up-regulates hypoxia-inducible factor-1 $\alpha$  transcription by involving phosphatidylinositol 3-kinase and nuclear factor kappaB in pulmonary artery smooth muscle cells. *Mol Biol Cell* 18: 4691–4697, 2007.
- Brauchle M, Funk JO, Kind P, and Werner S. Ultraviolet B and H<sub>2</sub>O<sub>2</sub> are potent inducers of vascular endothelial growth factor expression in cultured keratinocytes. *J Biol Chem* 271: 21793–21797, 1996.
- Brunelle JK, Bell EL, Quesada NM, Vercauteren K, Tiranti V, Zeviani M, Scarpulla RC, and Chandel NS. Oxygen sensing requires mitochondrial ROS but not oxidative phosphorylation. *Cell Metab* 1: 409–414, 2005.
- Cairns RA, Harris IS, and Mak TW. Regulation of cancer cell metabolism. *Nat Rev Cancer* 11: 85–95, 2011.
- Chan DA, Kawahara TL, Sutphin PD, Chang HY, Chi JT, and Giaccia AJ. Tumor vasculature is regulated by PHD2-mediated angiogenesis and bone marrow-derived cell recruitment. *Cancer Cell* 15: 527–538, 2009.
- Chandel NS, McClintock DS, Feliciano CE, Wood TM, Melendez JA, Rodriguez AM, and Schumacker PT. Reactive oxygen species generated at mitochondrial complex III stabilize hypoxia-inducible factor-1 $\alpha$  during hypoxia: a mechanism of O<sub>2</sub> sensing. *J Biol Chem* 275: 25130–25138, 2000.
- Choi JH, Kim TN, Kim S, Baek SH, Kim JH, Lee SR, and Kim JR. Overexpression of mitochondrial thioredoxin reductase and peroxiredoxin III in hepatocellular carcinomas. *Anticancer Res* 22: 3331–3335, 2002.
- Conrad M, Jakupoglu C, Moreno SG, Lippl S, Banjac A, Schneider M, Beck H, Hatzopoulos AK, Just U, Sinowatz F, Schmahl W, Chien KR, Wurst W, Bornkamm GW, and Brielmeier M. Essential role for mitochondrial thioredoxin reductase in hematopoiesis, heart development, and heart function. *Mol Cell Biol* 24: 9414–9423, 2004.
- Cummins EP, Berra E, Comerford KM, Ginouves A, Fitzgerald KT, Seeballuck F, Godson C, Nielsen JE, Moynagh P, Pouyssegur J, and Taylor CT. Prolyl hydroxylase-1 negatively regulates I $\kappa$ B kinase-beta, giving insight into hypoxia-induced NF $\kappa$ B activity. *Proc Natl Acad Sci U S A* 103: 18154–18159, 2006.
- D'Autreaux B and Toledano MB. ROS as signalling molecules: mechanisms that generate specificity in ROS homeostasis. *Nat Rev Mol Cell Biol* 8: 813–824, 2007.
- DeNicola GM, Karreth FA, Humpton TJ, Gopinathan A, Wei C, Frese K, Mangal D, Yu KH, Yeo CJ, Calhoun ES, Scrimieri F, Winter JM, Hruban RH, Iacobuzio-Donahue C, Kern SE, Blair IA, and Tuveson DA. Oncogene-induced Nrf2 transcription promotes ROS detoxification and tumorigenesis. *Nature* 475: 106–109, 2011.
- Drechsel DA and Patel M. Respiration-dependent H<sub>2</sub>O<sub>2</sub> removal in brain mitochondria via the thioredoxin/peroxiredoxin system. *J Biol Chem* 285: 27850–27858, 2010.
- Duyndam MC, Hulscher TM, Fontijn D, Pinedo HM, and Boven E. Induction of vascular endothelial growth factor expression and hypoxia-inducible factor 1 $\alpha$  protein by the oxidative stressor arsenite. *J Biol Chem* 276: 48066–48076, 2001.
- Gao P, Zhang H, Dinavahi R, Li F, Xiang Y, Raman V, Bhujwala ZM, Felsner DW, Cheng L, Pevsner J, Lee LA, Semenza GL, and Dang CV. HIF-dependent antitumorigenic effect of antioxidants *in vivo*. *Cancer Cell* 12: 230–238, 2007.
- Gerald D, Berra E, Frapart YM, Chan DA, Giaccia AJ, Mansuy D, Pouyssegur J, Yaniv M, and Mechta-Grigoriou

- F. JunD reduces tumor angiogenesis by protecting cells from oxidative stress. *Cell* 118: 781–794, 2004.
18. Ginouves A, Ilc K, Macias N, Pouyssegur J, and Berra E. PHDs overactivation during chronic hypoxia “desensitizes” HIF $\alpha$  and protects cells from necrosis. *Proc Natl Acad Sci U S A* 105: 4745–4750, 2008.
  19. Gorlach A, Diebold I, Schini-Kerth VB, Berchner-Pfannschmidt U, Roth U, Brandes RP, Kietzmann T, and Busse R. Thrombin activates the hypoxia-inducible factor-1 signaling pathway in vascular smooth muscle cells: role of the p22(phox)-containing NADPH oxidase. *Circ Res* 89: 47–54, 2001.
  20. Guzy RD, Hoyos B, Robin E, Chen H, Liu L, Mansfield KD, Simon MC, Hammerling U, and Schumacker PT. Mitochondrial complex III is required for hypoxia-induced ROS production and cellular oxygen sensing. *Cell Metab* 1: 401–408, 2005.
  21. Hanahan D and Weinberg RA. Hallmarks of cancer: the next generation. *Cell* 144: 646–674, 2011.
  22. Hanschmann EM, Lonn ME, Schutte LD, Funke M, Godoy JR, Eitner S, Hudemann C, and Lillig CH. Both thioredoxin 2 and glutaredoxin 2 contribute to the reduction of the mitochondrial 2-Cys peroxiredoxin Prx3. *J Biol Chem* 285: 40699–40705, 2010.
  23. Hellwig-Burgel T, Rutkowski K, Metzen E, Fandrey J, and Jelkmann W. Interleukin-1 $\beta$  and tumor necrosis factor- $\alpha$  stimulate DNA binding of hypoxia-inducible factor-1. *Blood* 94: 1561–1567, 1999.
  24. Huang LE, Arany Z, Livingston DM, and Bunn HF. Activation of hypoxia-inducible transcription factor depends primarily upon redox-sensitive stabilization of its  $\alpha$  subunit. *J Biol Chem* 271: 32253–32259, 1996.
  25. Ivan M, Kondo K, Yang H, Kim W, Valiando J, Ohn M, Salic A, Asara JM, Lane WS, and Kaelin WG, Jr. HIF $\alpha$  targeted for VHL-mediated destruction by proline hydroxylation: implications for O<sub>2</sub> sensing. *Science* 292: 464–468, 2001.
  26. Jaakkola P, Mole DR, Tian YM, Wilson MI, Gielbert J, Gaskell SJ, Kriegsheim A, Hebestreit HF, Mukherji M, Schofield CJ, Maxwell PH, Pugh CW, and Ratcliffe PJ. Targeting of HIF- $\alpha$  to the von Hippel-Lindau ubiquitylation complex by O<sub>2</sub>-regulated prolyl hydroxylation. *Science* 292: 468–472, 2001.
  27. Kamata H, Honda S, Maeda S, Chang L, Hirata H, and Karin M. Reactive oxygen species promote TNF $\alpha$ -induced death and sustained JNK activation by inhibiting MAP kinase phosphatases. *Cell* 120: 649–661, 2005.
  28. Land H, Parada LF, and Weinberg RA. Tumorigenic conversion of primary embryo fibroblasts requires at least two cooperating oncogenes. *Nature* 304: 596–602, 1983.
  29. Li L, Shoji W, Takano H, Nishimura N, Aoki Y, Takahashi R, Goto S, Kaifu T, Takai T, and Obinata M. Increased susceptibility of MER5 (peroxiredoxin III) knockout mice to LPS-induced oxidative stress. *Biochem Biophys Res Commun* 355: 715–721, 2007.
  30. Liou GY and Storz P. Reactive oxygen species in cancer. *Free Radic Res* 44: 479–496, 2010.
  31. Mandal PK, Schneider M, Kollé P, Kuhlencordt P, Forster H, Beck H, Bornkamm GW, and Conrad M. Loss of thioredoxin reductase 1 renders tumors highly susceptible to pharmacologic glutathione deprivation. *Cancer Res* 70: 9505–9514, 2010.
  32. Mannes AM, Seiler A, Bosello V, Maiorino M, and Conrad M. Cysteine mutant of mammalian GPx4 rescues cell death induced by disruption of the wild-type selenoenzyme. *FASEB J* 25: 2135–2144, 2011.
  33. Manning AM and Davis RJ. Targeting JNK for therapeutic benefit: from junk to gold? *Nat Rev Drug Discov* 2: 554–565, 2003.
  34. Mansfield KD, Guzy RD, Pan Y, Young RM, Cash TP, Schumacker PT, and Simon MC. Mitochondrial dysfunction resulting from loss of cytochrome c impairs cellular oxygen sensing and hypoxic HIF- $\alpha$  activation. *Cell Metab* 1: 393–399, 2005.
  35. Mecnovic J, Chowdhury R, Flashman E, and Schofield CJ. Use of mass spectrometry to probe the nucleophilicity of cysteinyl residues of prolyl hydroxylase domain 2. *Anal Biochem* 393: 215–221, 2009.
  36. Nonn L, Williams RR, Erickson RP, and Powis G. The absence of mitochondrial thioredoxin 2 causes massive apoptosis, exencephaly, and early embryonic lethality in homozygous mice. *Mol Cell Biol* 23: 916–922, 2003.
  37. Nytko KJ, Maeda N, Schlafl P, Spielmann P, Wenger RH, and Stiehl DP. Vitamin C is dispensable for oxygen sensing *in vivo*. *Blood* 117: 5485–5493, 2011.
  38. Pan Y, Mansfield KD, Bertozzi CC, Rudenko V, Chan DA, Giaccia AJ, and Simon MC. Multiple factors affecting cellular redox status and energy metabolism modulate hypoxia-inducible factor prolyl hydroxylase activity *in vivo* and *in vitro*. *Mol Cell Biol* 27: 912–925, 2007.
  39. Parrinello S, Samper E, Krtolica A, Goldstein J, Melov S, and Campisi J. Oxygen sensitivity severely limits the replicative lifespan of murine fibroblasts. *Nat Cell Biol* 5: 741–747, 2003.
  40. Perera RM and Bardeesy N. Cancer: when antioxidants are bad. *Nature* 475: 43–44, 2011.
  41. Pugh CW and Ratcliffe PJ. Regulation of angiogenesis by hypoxia: role of the HIF system. *Nat Med* 9: 677–684, 2003.
  42. Saitoh M, Nishitoh H, Fujii M, Takeda K, Tobiume K, Sawada Y, Kawabata M, Miyazono K, and Ichijo H. Mammalian thioredoxin is a direct inhibitor of apoptosis signal-regulating kinase (ASK) 1. *EMBO J* 17: 2596–2606, 1998.
  43. Sandin A, Dagnell M, Gonon A, Pernow J, Stangl V, Aspenstrom P, Kappert K, and Ostman A. Hypoxia followed by re-oxygenation induces oxidation of tyrosine phosphatases. *Cell Signal* 23: 820–826, 2011.
  44. Semenza GL. HIF-1 and tumor progression: pathophysiology and therapeutics. *Trends Mol Med* 8: S62–S67, 2002.
  45. Stanley BA, Sivakumaran V, Shi S, McDonald I, Lloyd D, Watson WH, Aon MA, and Paolocci N. Thioredoxin reductase-2 is essential for keeping low levels of H<sub>2</sub>O<sub>2</sub> emission from isolated heart mitochondria. *J Biol Chem* 286: 33669–33677, 2011.
  46. Tietze F. Enzymic method for quantitative determination of nanogram amounts of total and oxidized glutathione: applications to mammalian blood and other tissues. *Anal Biochem* 27: 502–522, 1969.
  47. Trachootham D, Alexandre J, and Huang P. Targeting cancer cells by ROS-mediated mechanisms: a radical therapeutic approach? *Nat Rev Drug Discov* 8: 579–591, 2009.
  48. Uhlen M, Oksvold P, Fagerberg L, Lundberg E, Jonasson K, Forsberg M, Zwahlen M, Kampf C, Wester K, Hober S, Wernerus H, Bjorling L, and Ponten F. Towards a knowledge-based Human Protein Atlas. *Nat Biotechnol* 28: 1248–1250, 2010.
  49. Valdman A, Haggarth L, Cheng L, Lopez-Beltran A, Montironi R, Ekman P, and Egevad L. Expression of redox pathway enzymes in human prostatic tissue. *Anal Quant Cytol Histol* 31: 367–374, 2009.

50. Vivanco I, Palaskas N, Tran C, Finn SP, Getz G, Kennedy NJ, Jiao J, Rose J, Xie W, Loda M, Golub T, Mellinghoff IK, Davis RJ, Wu H, and Sawyers CL. Identification of the JNK signaling pathway as a functional target of the tumor suppressor PTEN. *Cancer Cell* 11: 555–569, 2007.
51. Wang GL, Jiang BH, and Semenza GL. Effect of altered redox states on expression and DNA-binding activity of hypoxia-inducible factor 1. *Biochem Biophys Res Commun* 212: 550–556, 1995.
52. Xia C, Meng Q, Liu LZ, Rojanasakul Y, Wang XR, and Jiang BH. Reactive oxygen species regulate angiogenesis and tumor growth through vascular endothelial growth factor. *Cancer Res* 67: 10823–10830, 2007.
53. Zhong H, De Marzo AM, Laughner E, Lim M, Hilton DA, Zagzag D, Buechler P, Isaacs WB, Semenza GL, and Simons JW. Overexpression of hypoxia-inducible factor 1 $\alpha$  in common human cancers and their metastases. *Cancer Res* 59: 5830–5835, 1999.

Address correspondence to:

*Dr. Heike Beck*

*Walter Brendel Centre of Experimental Medicine  
Munich Heart Alliance  
Ludwig-Maximilians-University  
Marchioninstr. 15  
Munich 81377  
Germany*

*E-mail: heike.beck@med.uni-muenchen.de*

*Dr. Marcus Conrad*

*Helmholtz Zentrum München  
Institute of Developmental Genetics  
Ingolstädter Landstr. 1  
Neuherberg 85764  
Germany*

*E-mail: marcus.conrad@helmholtz-muenchen.de*

Date of first submission to ARS Central, February 19, 2014; date of final revised submission, January 7, 2015; date of acceptance, February 1, 2015.

#### Abbreviations Used

ASK-1 = apoptosis signal-regulating kinase 1  
BSO = L-buthionine sulfoximine  
DAPI = 4,6-diamidino-2-phenylindole  
DMSO = dimethyl sulfoxide  
DTT = dithiothreitol  
esiRNA = endoribonuclease-prepared small interfering RNA  
[Fe(II)] = ferrous iron  
[Fe(III)] = ferric iron  
GAPDH = glyceraldehyde 3-phosphate dehydrogenase  
GFP = green fluorescent protein  
grx2 = glutaredoxin-2  
GSH = reduced glutathione  
GSSG = oxidized glutathione  
H&E = hematoxylin-eosin  
H<sub>2</sub>O<sub>2</sub> = hydrogen peroxide  
Hif-1 $\alpha$  = hypoxia-inducible factor-1 $\alpha$   
HPLC = high-performance liquid chromatography  
JNK = c-Jun NH<sub>2</sub>-terminal Kinase  
KO = knockout  
LLC1 = Lewis lung carcinoma cells  
MEFs = mouse embryonic fibroblasts  
MKK4 = mitogen-activated protein kinase kinase 4  
NF- $\kappa$ B = nuclear factor- $\kappa$ B  
*Nrf2* = NF-E2-related factor-2  
PBS = phosphate-buffered solution  
PEG-catalase = polyethylene glycol-conjugated catalase  
PHD = Hypoxia-inducible factor prolyl hydroxylase  
PI = proliferation index  
Prx III = peroxiredoxin III  
PTP = protein tyrosine phosphatase  
qRT-PCR = quantitative real-time-polymerase chain reaction  
ROS = reactive oxygen species  
SD = standard deviation  
Txn2 = mitochondrial thioredoxin  
Txnrd2 = mitochondrial thioredoxin reductase  
VEGF-A = vascular endothelial growth factor A  
WT = wildtype